ACS APPLIED MATERIALS & INTERFACES

Research Article

www.acsami.org

Facile Synthesis of Dendritic Gold Nanostructures with Hyperbranched Architectures and Their Electrocatalytic Activity toward Ethanol Oxidation

Jianshe Huang, Xinyi Han, Dawei Wang, Dong Liu, and Tianyan You*

State Key Laboratory of Electroanalytical Chemistry, Changchun Institute of Applied Chemistry, Chinese Academy of Sciences, Changchun, Jilin 130022, People's Republic of China

Supporting Information

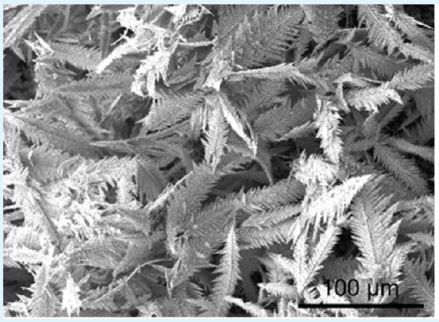

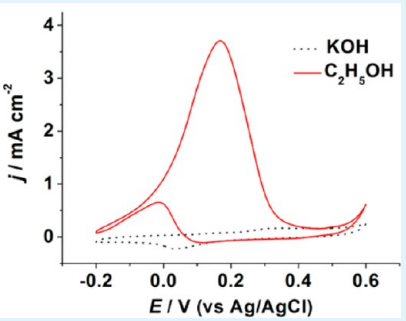

ABSTRACT: Gold dendritic nanostructures with hyperbranched architectures were synthesized by the galvanic replacement reaction between nickel wire and $HAuCl_4$ in aqueous solution. The study revealed that the morphology of the obtained nanostructures strongly depended on experimental parameters such as the $HAuCl_4$ solution concentration, reaction temperature, and time, as well as stirring or not. According to the investigation of the growth process, it was proposed that gold nanoparticles with rough surfaces were first deposited on the nickel substrate and that subsequent growth preferentially occurred on the preformed gold nanoparticles, finally leading to the formation of hyperbranched gold dendrites via a self-organization process under nonequilibrium conditions. The electrochemical experiment results demonstrated that the as-obtained gold dendrites exhibited high catalytic activity toward ethanol electrooxidation in alkaline solution, indicating that this nanomaterial may be a potential catalyst for direct ethanol fuel cells.

KEYWORDS: *gold dendritic nanostructures, galvanic replacement reaction, nickel wire, ethanol electrooxidation*

1. INTRODUCTION

The fabrication of gold (Au) nanostructures with novel morphologies has been an active research area because of their morphology-dependent optical, electronic, and catalytic properties and promising applications.[1,2] Among various morphologies, dendritic nanostructures have attracted much attention because of their importance in understanding the fascinating fractal growth phenomena[3] and their potential applications in photoluminescence,[4] surface-enhanced Raman spectroscopy (SERS),[5−8] superhydrophobic surfaces,[8,9] sensor/biosensors,[10,11] catalysis,[12,13] and electrocatalysis.[8,14−17] Furthermore, the fabrication of nanostructures with hierarchical architectures is a crucial step in bridging the gap between nanoscaled building blocks and complex functional materials and devices. It has been documented that nonequilibrium growth and molecular anisotropy played important roles in the formation of dendritic nanostructures.[3,18] Because of the highly symmetric face-centered-cubic (fcc) crystal structure of Au, it is usually needed to create a nonequilibrium growth condition for the preparation of Au dendritic structures by adjusting reaction conditions such as the solvent, reactant concentration, additive, temperature, convection, etc. To date, many methods have been developed for the preparation of Au dendritic nanostructures, including electrodeposition,[8−11,15−17] a wet-chemical route,[7,13,14,19,20] a seeded growth method,[21−23] an aqueous/organic interfacial reaction,[5,24] a hydrothermal reduction method,[6] a template method,[25] and curing of spin-coated Au colloids at elevated temperatures.[26] These methods provided new avenues to study the growth process of dendritic structures, and the obtained products exhibited some promising applications. However, surfactants, polymers, or certain ionic species are usually required in these approaches as shape-directing agents by preferential adsorption on specific crystal planes to form anisotropic nanostructures. The adsorbed heterogeneous impurities on the obtained nanostructure surface will greatly interfere with their practical applications in SERS, sensing, and catalysis. Therefore, it would be highly desirable to develop a facile and effective method to synthesize

Received: June 29, 2013
Accepted: August 25, 2013
Published: August 25, 2013

Au dendritic nanostructures with "clean" surfaces and hyperbranched architectures.

The galvanic replacement reaction provides a remarkably simple and versatile route to preparing various metal nanostructures, in which the driving force is the difference in the standard electrode potential between the deposited metal and sacrificial substrate. This method was also known as transmetalation, which was first applied by Adžić's group[27,28] and Buess-Herman's group[29,30] to spontaneously deposit noble metal [e.g., platinum (Pt), palladium (Pd), silver (Ag)] via displacement of a copper (Cu) adlayer on flat electrode substrates. Similarly, Sotiropoulos and co-workers[31,32] prepared Pt−nickel (Ni) bimetallic nanostructures by using the similar method, whereby a controlled amount of Ni was electrodeposited onto the electrode surface and subsequently partially exchanged for Pt upon immersion of the Ni-modified electrode into a H_2PtCl_6 solution. In this spontaneous reaction, no external current source or any reducing agent is needed. Recently, the galvanic replacement reaction was extensively studied in the preparation of Au dendritic structures.[12,33−37] Numerous metals or semiconductors, such as Ag, zinc (Zn), aluminum (Al), Cu, iron (Fe), and silicon (Si), are usually used as substrates to fabricate noble-metal dendrites. The standard redox potential of Ni^{2+}/Ni (−0.257 V vs SHE, 25 °C) is lower than those of noble metallic ions.[38] Therefore, Ni metallic wire or foil can also be used as a sacrificial substrate to prepare noble-metal nanostructures. For example, porous metal nanorods (Au, Pt, and Pd) and Pt nanotubes were synthesized through a spontaneous galvanic replacement reaction between Ni nanorods and noble-metal precursors.[39,40] Ni@Au composite materials were also prepared via the galvanic replacement reaction using prickly Ni nanowires as templates.[41] In the case of dendritic nanostructures, Xiao and co-workers[42] obtained Pd and Ag dendritic nanostructures by using Raney Ni as the template and reducing agent with the assistance of ultrasonic waves. Bai et al.[37] prepared Au dendritic nanostructures with a few branches and relatively rough structures on a Ni foil substrate in the mixture solution of ethanol/water containing ionic liquid [camphorC_2mim]Cl. To the best of our knowledge, there is no report on the synthesis of Au dendritic nanostructures using a Ni substrate in aqueous solution without any additive and template.

In this paper, we developed a facile and efficient method to prepare Au dendritic nanostructures with hyperbranched architectures via the galvanic replacement reaction between commercial Ni wire and $HAuCl_4$ in aqueous solution at room temperature. The advantages of this novel method for the preparation of Au dendrites include the following: (1) It is a templateless process. (2) No surfactant, polymer, and other additives were involved in the reaction. (3) A pure aqueous solution was employed as the reaction medium. (4) The as-obtained nanostructure with a "clean" surface could be directly used as the catalyst without any pretreatment. Because of the clean surfaces and advantages of dendritic nanostructures (large surface area and abundant active sites), it has been shown that the obtained Au dendrites could be used as electrocatalysts and exhibited high catalytic activity toward ethanol oxidation in an alkaline medium.

2. EXPERIMENTAL SECTION

2.1. Materials. Tetrachloroauric acid tetrahydrate ($HAuCl_4{\cdot}4H_2O$, AR) was purchased from Shanghai Chemistry Co., Ltd. (China). Ni wire (0.5 mm diameter, 99.99%) was obtained from Alfa Aesar. Ammonia solution (25%), ethanol (C_2H_5OH), and potassium hydroxide (KOH) were purchased from Beijing Chemical Factory (Beijing, China). All chemicals were used without further purification. The water used throughout the experiments was double-distilled water.

2.2. Synthesis of Au Dendritic Nanostructures. Commercial Ni wire was immersed in a 25% ammonia solution for 30 min to remove the thin surface nickel oxide film and then sonicated in water for a few minutes prior to the galvanic replacement reaction. In a typical synthesis, the previously cleaned Ni wire was immersed into 1 mL of a 10 mM $HAuCl_4$ solution in a 1.5 mL centrifuge tube. The reaction was performed at room temperature (25 °C) without perturbation and lasted for 6 h. Upon completion of the synthesis, the Ni wire was removed from the $HAuCl_4$ solution and rinsed with water for 3 min.

2.3. Apparatus. The morphology and composition of the products were acquired using a FEI XL30 ESEM FEG scanning electron microscope equipped with energy-dispersive X-ray analyzer at an accelerating voltage of 20 kV. High-resolution transmission electron microscopy (HRTEM) and selected-area electron diffraction (SAED) studies were performed on a Philips-FEI Tecnai F20 microscope (Philips, The Netherlands) at an accelerating voltage of 200 kV. UV−vis absorption spectra were recorded with a Cary 50 UV−vis spectrophotometer (Varian, USA). X-ray diffraction (XRD) analysis was carried out on a D8 ADVANCE X-ray diffractometer using Cu (40 kV, 40 mA) radiation over a range of 20−80°. For XRD analysis and UV−vis spectral measurement, Au nanostructures were separated from Ni wire by ultrasonic treatment in water and then washed three times and redispersed in water. Inductively coupled plasma optical emission spectrometry (ICP-OES) was conducted on IRIS Intrepid XSP (Thermo Fisher). Cyclic voltammetric (CV) experiments were performed with a CHI 832 electrochemical analyzer (CH Instruments, Chenhua Co., Shanghai, China). A conventional three-electrode system was used, including a Ag/AgCl (saturated KCl) electrode as the reference electrode, a Pt wire as the counter electrode, a polycrystalline Au electrode or Au-dendrite-modified glassy carbon (GC) electrode as the working electrode.

2.4. Electrochemical Experiments. GC (⌀ = 3 mm) electrodes were successively polished with 0.3 and 0.05 μm alumina powder and then were ultrasonically cleaned in water and ethanol for 10 min. A total of 5 μL of a Au dendrite solution was dropped on the clean GC electrode surface and allowed to dry naturally in air. Then, 2 μL of 0.05 wt % Nafion in ethanol was used to fix the catalysts and dried before electrochemical experiments. For comparison, a commercial polycrystalline Au electrode was mechanically cleaned, electrochemically activated in a 0.5 M H_2SO_4 solution, and then used for electrochemical experiments. Ethanol electrooxidation measurements were performed in a 1.0 M KOH solution containing 1.0 M ethanol. All solutions were deaerated by bubbling nitrogen for 30 min prior to electrochemical measurement.

3. RESULTS AND DISCUSSION

3.1. Characterization of the Au Dendritic Nanostructures. In this work, Ni wire was employed as the substrate to synthesize Au nanostructures in aqueous solution at room temperature (25 °C). The standard electrode potential of a $AuCl_4^-$/Au pair (1.002 V vs SHE, 25 °C) is much higher than that of a Ni^{2+}/Ni pair (−0.257 V vs SHE).[38] Therefore, $HAuCl_4$ can be reduced by Ni, as shown in following equation:

$$3Ni(s) + 2AuCl_4^-(aq) \rightarrow 2Au(s) + 3Ni^{2+}(aq) + 8Cl^-(aq) \quad (1)$$

Figure 1 shows the typical scanning electron microscopy (SEM) images of the Au dendrites with different magnifications obtained from a standard synthetic process. As shown in Figure 1a, the as-obtained products consist exclusively of uniform plumelike dendrites with an average length of 65 μm. Close

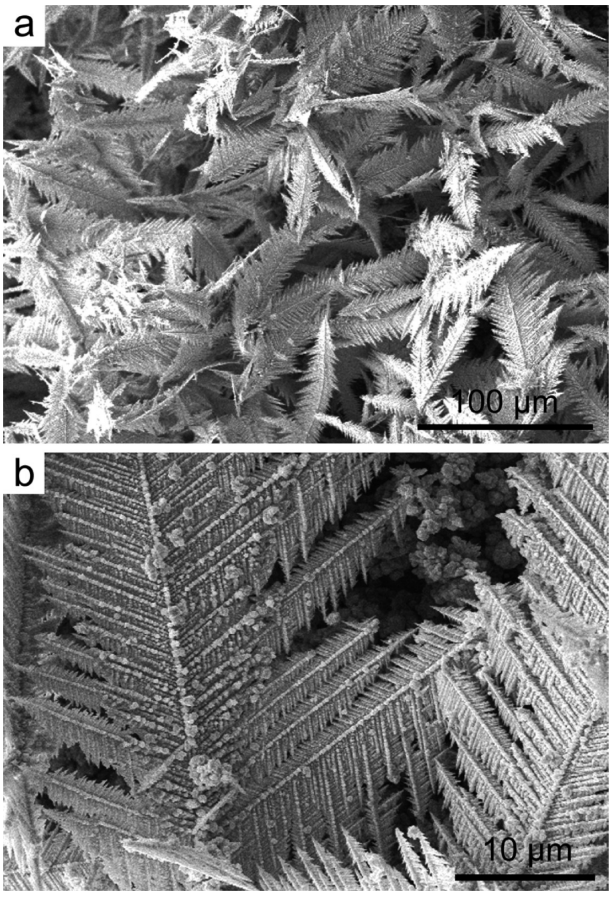

Figure 1. SEM images of the as-prepared Au dendrites with different magnifications.

inspection of the dendrites under higher magnification (Figure 1b) reveals that the hyperbranched dendrites show a hierarchical structure composed of a trunk, branches (secondary branch), and leaves (tertiary branch). The multilevel branches preferentially grow along two definite directions rather than randomly ramified growth, which emerges at 60° angles with respect to their corresponding central backbone. These branches in each row have a uniform spacing and are parallel to each other. This special morphology implied that the Au dendritic structures grew along a preferential direction.

HRTEM and SAED analyses were carried out to determine the crystal orientation and growth direction of Au dendrites (Figure 2). Figure 2a shows the TEM image of an undeveloped

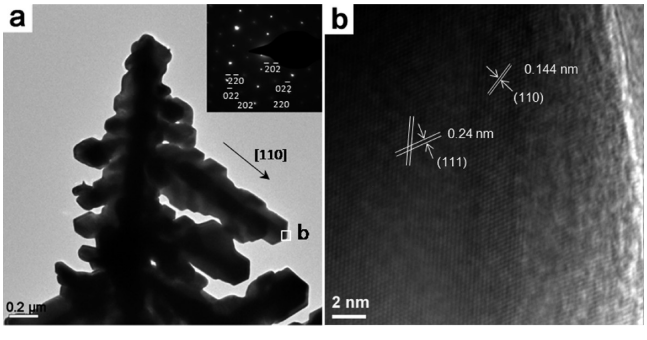

Figure 2. (a) TEM images of the Au dendrites (inset: SAED pattern of Au in the white square region). (b) HRTEM image of the tip of the branch marked in part a.

Au dendrite, which can be used to determine the growth direction of a Au dendrite. HRTEM and SAED images were recorded at the thin tip of a branch. The SAED pattern (inset in Figure 2a) exhibits clear diffraction spots indexed to the $[\bar{1}11]$ zone axis of the fcc Au single crystal, indicating that the branches of the Au dendrites are single-crystalline grown along the ⟨110⟩ direction. HRTEM measurements also demonstrated this single-crystalline nature of the Au dendrite at the tip areas of the branch, as shown in Figure 2b. The atomic lattice exhibits a *d* spacing of 0.144 nm in the axial direction of the branch, consistent with the *d* spacing of (110) planes for the fcc Au crystal, which further confirms the ⟨110⟩ growth direction of the branch.

The chemical composition of the dendrites was determined by energy-dispersive X-ray (EDX) analysis. Except for the Si signal originating from the indium−tin oxide substrate, the EDX spectrum shows only Au signals (Figure 3a), indicating

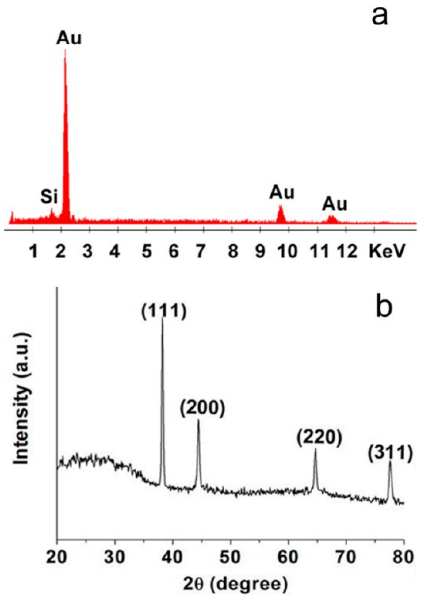

Figure 3. EDX (a) and XRD (b) patterns of the as-prepared Au dendrites.

that the dendrites consisted of pure Au. XRD analysis (Figure 3b) was used to evaluate the overall purity and crystal structure of the Au dendrites. Four sharp diffraction peaks located at 38.2, 44.4, 64.7, and 77.6° are indexed to the [111], [200], [220], and [311] diffraction peaks of the fcc metallic Au (JCPDS no. 04-0784), respectively, confirming that the dendrites are pure and well-crystallized Au crystals. The intensity ratios of the (111) plane to the (200) and (220) planes are 2.6 and 4.1, respectively. These values are higher than those of the polycrystalline Au (1.89 and 3.1; JCPDS no. 04-0784). These observations indicated that the as-prepared Au dendrites had a tendency to grow preferentially along the ⟨110⟩ direction, which was dominated by the lowest-energy plane (111).[17]

The UV−vis spectra of Au nanostructures strongly depend on their shape, size, and aspect ratio.[43] In our experiment, the UV−vis spectra of Au nanostructures changed with elongation of the reaction time. At the initial reaction stage (0.5 h), the obtained Au nanoparticles showed a single Au surface plasmon resonance (SPR) peak at about 550 nm. As the reaction proceeded, the Au SPR peak broadened and the location was

red-shifted. Finally, the UV−vis spectrum of Au dendrites displayed a gradual increase in absorption from about 500 nm to the near-IR region (Figure S1 in the Supporting Information, SI). It is well-known that anisotropic Au nanoparticles normally exhibit two principal SPR peaks (transverse and longitudinal bands). The gradual increase in absorption could be ascribed to the longitudinal plasmon band. This result indicated a remarkable overlapping between the transverse and longitudinal bands.[7] The observed unusual overlapping between the transverse and longitudinal bands might be ascribed to a variety of sizes, aspect ratios, and various couplings between the trunks and branches of the obtained Au dendrites.

3.2. Effect of the Reaction Conditions. *3.2.1. $HAuCl_4$ Solution Concentration.* It was found that $HAuCl_4$ solution concentrations remarkably influenced the morphologies of the as-prepared Au nanostructures. Figure 4 presents SEM images

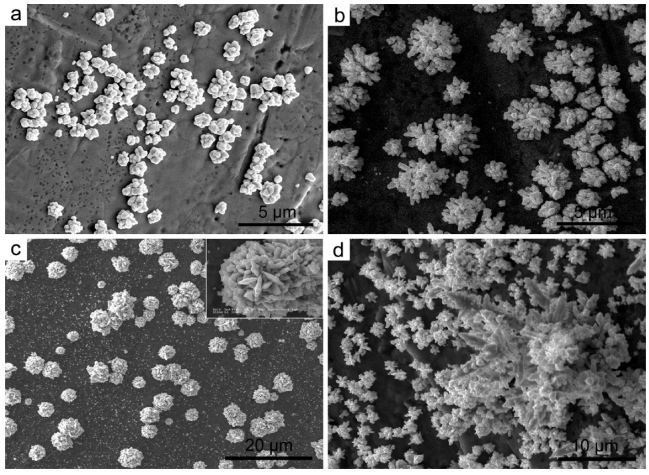

Figure 4. SEM images of the samples synthesized at different $HAuCl_4$ solution concentrations: (a) 0.1 mM; (b) 0.5 mM; (c) 1.0 mM; (d) 5.0 mM.

of the products synthesized with different $HAuCl_4$ concentrations (0.1−5 mM). When a 0.1 mM $HAuCl_4$ solution was used, many multiped Au nanostructures with nonuniform size were obtained (Figure 4a). An increase of the concentration of the $HAuCl_4$ solution to 0.5 mM resulted in dendritic nanoparticles with 1−3 μm in size, and the branch of the nanostructures was elongated and increased in number (Figure 4b). However, when a 1.0 mM $HAuCl_4$ solution was used, the obtained samples changed to three-dimensional microspheres with flowerlike structure (Figure 4c). The average diameter of the microsphere was 4.5 μm. Close inspection showed that the microspheres were composed of many two-dimensional nanoflakes or one-dimensional nanopricks, which self-assembled into a three-dimensional hierarchical structure (Figure 4c, inset). Interestingly, when the $HAuCl_4$ solution concentration was increased to 5.0 mM, the as-prepared products changed into dendritic morphology, including small monodisperse bare dendrites and big aggregated dendrites (Figure 4d). The small dendrites are bare and without any secondary branch. At the same time, some large dendrites with not fully grown multibranches appeared. Upon a further increase of the $HAuCl_4$ solution concentration to 10.0 mM, the perfect hyperbranched Au dendrites were obtained (Figure 1). These results indicated that the $HAuCl_4$ solution concentration played an important role in the formation of Au dendrites and a higher $HAuCl_4$ concentration facilitated the formation of dendritic nanostructures. Additionally, the formation of large Au dendrites was not monotonously growing from small fractal Au nanostrucutres with an increase of the $HAuCl_4$ solution concentration. It has been documented that an increase in the reactant concentration would lead to an enhanced reaction rate and thus a nonequilibrium condition being easily built, which was beneficial to the preparation of dendritic structures.[44]

3.2.2. Reaction Temperature. Besides the $HAuCl_4$ solution concentration, a proper reaction temperature is also necessary for the formation of Au dendrites. Figure S2 (in the SI) shows SEM images of the products obtained at different reaction temperatures. At 50 °C, a large number of rough Au dendrites were synthesized on the substrate, which showed poor symmetry and contained some random-shaped nanoparticles on the surface (Figure S2a in the SI). Furthermore, the hiberarchy of the multilevel branches could not be clearly distinguished. When the reaction temperature was further increased to 100 °C, many aggregated nanoparticles were formed and no dendrites could be observed (Figure S2b in the SI). These observations demonstrated that the reaction temperature also has a considerable effect on the morphologies of the as-prepared nanostructures, and a proper reaction temperature is critical to the formation of hyperbranched dendrites.

3.2.3. Stirring and Reaction Time. To study the possible growth mechanism of Au dendrites, we also investigated the effect of stirring and the reaction time on the morphologies of the obtained nanostructures (Figure 5). Figure 5a shows the

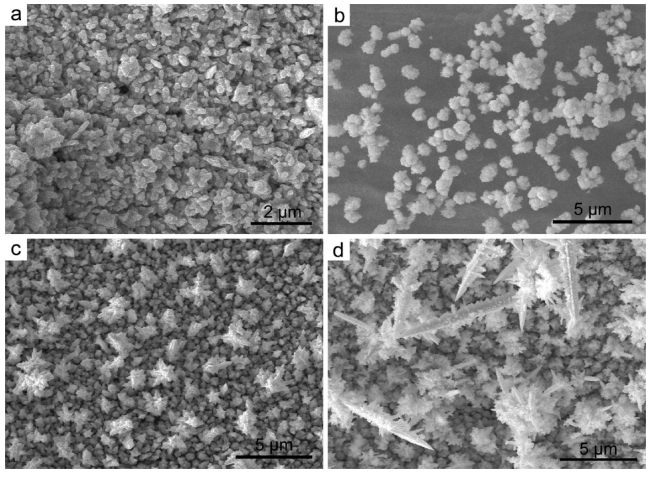

Figure 5. SEM images of the products obtained under stirring for 6 h (a) and without stirring for 0.5 h (b), 1.5 h (c), and 3 h (d).

SEM image of the products synthesized with stirring and other conditions remaining constant as the typical synthesis process. It can be clearly observed that the products are composed of many random-shaped nanoparticles, indicating that keeping the solution undisturbed is critical to the formation of Au dendrites. The reason may be ascribed to the fact that stirring created the current equilibrium condition and destroyed the nonequilibrium growth conditions for dendritic nanostructures.[45] Figure 5b illustrates the SEM image of the samples obtained at 0.5 h without stirring. Au nanoparticles with rough surfaces were deposited on the substrate. Then these nanoparticles served as nucleation sites for the further growth of anisotropic Au dendritic nanostructures. When the reaction time was

prolonged to 1.5 h, a few undeveloped Au dendrites appeared in some areas of the substrate (Figure 5c). The dendrites continuously grew to form nanostructures with a micrometer-sized trunk and undeveloped branches for a reaction time of 3 h (Figure 5d). Finally, three-dimensional Au dendritic nanostructures with hyperbranched architectures could be obtained for a reaction time of 6 h (Figure 1).

3.2.4. Possible Growth Mechanism of Au Dendrites. Scheme 1 illustrated the growth mechanism and process of Au dendrites. The galvanic replacement reaction between Ni and $HAuCl_4$ (eq 1) first took place spontaneously on the Ni wire surface through a direct surface reaction, which produced small Au nanoparticles on the substrate as nuclei. After that, a primary cell with a Ni wire as the anode and Au nanoparticles as the cathode was formed. Subsequent growth of Au nanostructures would preferentially occur on the preformed Au nuclei because of the relatively high activation energy for the surface reaction. With the progress of the primary cell reaction, Ni substrate was continuously consumed and Au nanostructures grew gradually. Finally, Au nanostructures with hyperbranched architectures could be obtained through a self-organization process under nonequilibrium conditions.[46]

Scheme 1. Schematic Presentation of the Growth Mechanism and Process of Au Dendrites

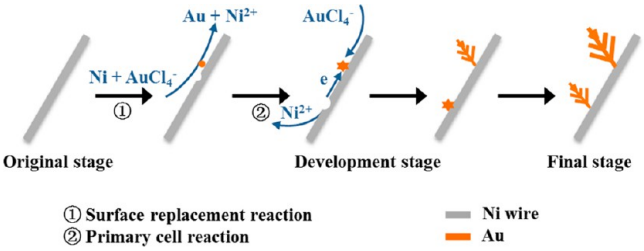

It has been reported that a delicate balance between the diffusion and reaction rates was responsible for the formation of Au dendrites.[36] Therefore, a subtle variation of the reaction parameters (e.g., reactant concentration, temperature, and stirring), which influences the diffusion and reaction rates, will result in a great change of the morphology of the obtained nanostructures. As shown in our experiment, the lower $HAuCl_4$ concentration provided a slow reaction rate, and only fractal nanostructures and undeveloped dendrites were produced (Figure 4). An increase of the reaction temperature greatly enhanced the diffusion and reaction rates, which led to the formation of poor dendritic structures and aggregated nanoparticles (Figure S2 in the SI). The higher the reaction temperature was, the farther the distance deviated from the proper condition for the dendrite growth. While the stirring speeded up the diffusion and destroyed the nonequilibrium conditions, the obtained products were not dendrites but random-shaped nanoparticles (Figure 5a). Therefore, the perfect Au dendritic nanostructures could only be obtained when the reaction was conducted under the conditions of 10 mM $HAuCl_4$ at room temperature (25 °C) without stirring. Additionally, the metal substrate and reaction medium may also play important roles in the formation of dendritic nanostructures. Qin et al.[36] found that Ni could not be used as an effective metal substrate for the deposition of Au crystals from $HAuCl_4$ solutions in ionic liquid $[BMIM][PF_6]$. Bai and coworkers[37] obtained Au dendritic nanostructures with many defects when Ni was used as the substrate, and the reaction was conducted in an ethanol/water mixture solution containing $[camphorC_2mim]Cl$. The reason may be ascribed to the slower reaction rate in the ionic liquid medium than that in aqueous solution. If the metal with relatively high reactivity, e.g., Zn, was used as the substrate, AuZn alloy dendrites rather than metal Au dendrites were obtained in aqueous solution.[36] In our experiment, well-matched reaction and diffusion rates were obtained; thus, perfect Au dendrites could be produced by using Ni as the substrate and aqueous solution as the reaction medium. Therefore, the developed method provided a facile and efficient route to preparing Au dendrites in aqueous solution without any additive.

3.3. Electrocatalytic Activity of Au Dendrites toward Ethanol Oxidation. Direct alcohol fuel cells have attracted enormous research attention as a clean energy conversion device because of their much higher available energy density and ease of handling of liquid fuels. In particular, ethanol has received considerable interest because of its lower toxicity than methanol and the fact that it can be produced in large quantities through the fermentation of biomass.[47] Precious metal Pt is the most extensively used catalyst in the electrocatalytic oxidation of ethanol. However, the major problem associated with the Pt-based catalysts is catalyst poisoning by adsorbed CO-like species generated during the oxidation process.[48] Au has been known as an active electrode material for the oxidation of ethanol for a long time.[49−51] In recent years, various nanostructured Au electrodes were also utilized for the electrocatalytic oxidation of ethanol and exhibited high activity.[8,15,52−54] However, alkaline conditions are considered to be an important prerequisite for efficient aqueous-phase Au electrocatalysis. Because Au is much less prone to the formation of poisoning oxides, the activity of Au in an alkaline medium can be very high, even higher than that of Pt.[55] Therefore, the catalytic activity of the as-prepared Au dendrites was evaluated for the electrooxidation of ethanol under alkaline conditions because of their specific hyperbranched morphology.

The as-prepared Au dendrites were deposited onto a cleaned GC electrode to prepare Au-dendrite-modified electrode. Figure S3 (in the SI) shows cyclic voltammograms of the Au-dendrite-modified electrode and a commercial polycrystalline Au electrode (poly-Au) in a 0.5 M H_2SO_4 solution. The cyclic voltammograms exhibited the typical behavior of a Au electrode in an acid medium, with clear peaks of the formation and subsequent reduction of the gold oxides. It was found that the morphology of the Au dendrites on the electrode was retained after continuous potential cycling of more than 100 times. The electrochemically active surface area (EASA) was calculated from the charge consumed during the reduction of surface oxides using the value of 400 $\mu C/cm^2$ for a clean Au electrode.[56] The current values were all normalized to the EASA to obtain the current density. For the Au-dendrite-modified electrode, the measured EASA was 0.066 cm^2, which was nearly twice that of the poly-Au electrode (0.034 cm^2). The larger surface area was attributed to the hyperbranched structure of Au dendrites and expected to enhance the electrocatalytic activity.

According to the literature,[55] the electrooxidation of ethanol to aldehyde involved the transfer of two protons and two electrons through the following reactions:

$$CH_3CH_2OH \rightleftharpoons CH_3CH_2O^- + H^+ \quad (2)$$

$$CH_3CH_2O^- \rightarrow CH_3CH{=}O + H^+ + 2e^- \quad (3)$$

In reaction (2), deprotonation of ethanol is base-catalyzed, with no need for a Au catalyst (solution-mediated step). Once the reactive alkoxide intermediate is formed, it will quickly eliminate the second proton with Au as electron acceptor (Au-catalyzed step). Aldehydes are not stable in alkaline solution and will react further to produce acetic acid. Recent density functional theory calculations also suggested that an OH group adsorbed onto Au significantly lowered the barrier for the second proton elimination.[57] Therefore, the electrocatalytic activity of Au dendrites toward ethanol oxidation was evaluated in different concentrations of a KOH solution. As shown in Figure S4 in the SI, the current density increased nonlinearly from 0.94 to 2.89 mA/cm^2 with an increase of the KOH concentration; accordingly, the peak potential negatively shifted from 0.37 to 0.15 V. These results indicated that the KOH concentration (i.e., pH value) greatly influenced the electrocatalytic activity of Au dendrites. It also testified that the solution hydroxide promoted the initial deprotonation, which is the important first step of the overall oxidation reaction.

Figure 6a shows typical cyclic voltammograms of the Au-dendrite-modified electrode in 1.0 M KOH solutions with

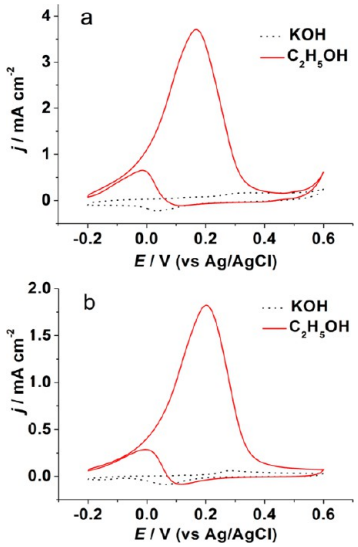

Figure 6. Cyclic voltammograms of a Au-dendrite-modified GC electrode (a) and a polycrystalline Au electrode (b) in 1.0 M KOH solutions with (solid line) and without (dotted line) 1.0 M ethanol. Scan rate: 50 mV/s.

(solid line) and without (dotted line) 1.0 M ethanol. In the absence of ethanol, the CV curve exhibited a broad oxidation peak in the region of 0.3−0.4 V, which was ascribed to the formation of Au surface oxides, and the reduction peak appearing at 0−0.1 V was attributed to the subsequent removal of the oxides.[8] When 1.0 M ethanol was added, a huge oxidation peak could be observed at 0.17 V, which may be ascribed to the oxidation of ethanol to acetate through a four-electron-transfer reaction,[50] indicating the high electrocatalytic activity of the Au dendrites. During the negative-going potential sweep, a new anodic peak appeared at about 0 V, and the onset oxidation potential (0.1 V) coincided with that of gold oxide reduction in the ethanol-free KOH solution. This result indicated that the active Au surface immediately recovered after the removal of gold oxides. As a comparison, the electrocatalytic activity of the poly-Au electrode was also evaluated under identical conditions. As shown in Figure 6b, with the addition of 1.0 M ethanol, the poly-Au electrode showed an oxidation peak at about 0.22 V, which is 50 mV more positive than that of the Au-dendrite-modified electrode. Moreover, the anodic peak current density at the poly-Au electrode was calculated to be 0.99 mA/cm^2, which is less than half that at the Au-dendrite-modified electrode (2.05 mA/cm^2). These results demonstrated that the Au dendrite electrode has a considerably higher electrocatalytic activity for ethanol oxidation compared to the poly-Au electrode. The mass-specific activity of Au dendrites toward ethanol electrooxidation was also calculated based on ICP-OES measurements. The current density of 137.4 mA/mg$_{Au}$ was obtained. This value is smaller than that of 4 nm Au nanoparticles supported on an activated carbon (Au/C) catalyst (about 300 mA/mg$_{Au}$),[58] which may be due to the large size of Au dendrites in our experiment. The electrocatalytic activity of metal nanostructures strongly depends on their composition, shape, and size and is influenced by the capping agents and other surface impurities.[59,60] In the case of Au dendrites, the EDX spectrum (Figure 3a) indicated that the dendrites consisted of pure Au. Therefore, we speculated that the high electrocatalytic activity could be related to the "clean" surface and hyperbranched morphology of the Au dendrites, which provided a large surface area and numerous active sites (e.g., kink or step sites). Furthermore, the exposed surface of Au dendrites with specific crystal planes could also contribute to the observed high electrocatalytic activity.

4. CONCLUSIONS

In summary, three-dimensional Au dendritic nanostructures with hyperbranched architectures were synthesized by using the spontaneous galvanic replacement reaction between Ni wire and $HAuCl_4$ in aqueous solution at room temperature. It was shown that the hyperbranched dendrites have a hierarchical structure composed of a trunk, branches, and leaves. The experimental results demonstrated that the $HAuCl_4$ solution concentration, reaction temperature, and time and stirring or not played key roles in the formation of Au dendrites. Under proper conditions, well-matched reaction and diffusion rates were obtained, leading to the formation of hyperbranched dendrites through a self-organization process under non-equilibrium conditions. Electrochemical experiments suggested that the obtained Au dendrites exhibited high electrocatalytic activity toward ethanol oxidation, which may be related to the unique hyperbranched nanostructures. This synthetic method is simple, effective, and low-cost and is anticipated to be applicable to the fabrication of other metal nanostructured materials, which could find promising applications in catalysis, biosensing, and nanodevices.

■ ASSOCIATED CONTENT

Supporting Information

UV−vis absorption spectrum of the as-prepared Au dendrites (Figure S1), SEM images of the samples synthesized at different reaction temperatures (Figure S2), cyclic voltammograms of a Au-dendrite-modified GC electrode and a polycrystalline Au electrode in 0.5 M H_2SO_4 (Figure S3), and cyclic voltammograms of a Au-dendrite-modified GC electrode in different concentrations of a KOH solution with 1.0 M ethanol (Figure S4). This material is available free of charge via the Internet at http://pubs.acs.org.

AUTHOR INFORMATION

Corresponding Author

*E-mail: youty@ciac.jl.cn. Tel. and Fax: +86-431-85262850.

Notes

The authors declare no competing financial interest.

ACKNOWLEDGMENTS

We gratefully acknowledge financial support from the National Natural Science Foundation of China (Grants 21105098 and 21222505).

REFERENCES

(1) Grzelczak, M.; Perez-Juste, J.; Mulvaney, P.; Liz-Marzan, L. M. *Chem. Soc. Rev.* **2008**, *37*, 1783−1791.
(2) Zhu, Z.; Meng, H.; Liu, W.; Liu, X.; Gong, J.; Qiu, X.; Jiang, L.; Wang, D.; Tang, Z. *Angew. Chem., Int. Ed.* **2011**, *50*, 1593−1596.
(3) Ben-Jacob, E.; Garik, P. *Nature* **1990**, *343*, 523−530.
(4) Hu, Y.; Pan, N.; Zhang, K.; Wang, Z.; Hu, H.; Wang, X. *Phys. Status Solidi A* **2007**, *204*, 3398−3404.
(5) Lu, G.; Li, C.; Shi, G. *Chem. Mater.* **2007**, *19*, 3433−3440.
(6) Tang, X.-L.; Jiang, P.; Ge, G.-L.; Tsuji, M.; Xie, S.-S.; Guo, Y.-J. *Langmuir* **2008**, *24*, 1763−1768.
(7) Huang, T.; Meng, F.; Qi, L. *Langmuir* **2010**, *26*, 7582−7589.
(8) Ye, W.; Yan, J.; Ye, Q.; Zhou, F. *J. Phys. Chem. C* **2010**, *114*, 15617−15624.
(9) Zhang, X.; Shi, F.; Yu, X.; Liu, H.; Fu, Y.; Wang, Z.; Jiang, L.; Li, X. *J. Am. Chem. Soc.* **2004**, *126*, 3064−3065.
(10) Huan, T. N.; Ganesh, T.; Kim, K. S.; Kim, S.; Han, S.-H.; Chung, H. *Biosens. Bioelectron.* **2011**, *27*, 183−186.
(11) Li, F.; Han, X.; Liu, S. *Biosens. Bioelectron.* **2011**, *26*, 2619−2625.
(12) Ye, W.; Chen, Y.; Zhou, F.; Wang, C.; Li, Y. *J. Mater. Chem.* **2012**, *22*, 18327−18334.
(13) Huang, D.; Bai, X.; Zheng, L. *J. Phys. Chem. C* **2011**, *115*, 14641−14647.
(14) Han, X.; Wang, D.; Huang, J.; Liu, D.; You, T. *J. Colloid Interface Sci.* **2011**, *354*, 577−584.
(15) Feng, J.-J.; Li, A.-Q.; Lei, Z.; Wang, A.-J. *ACS Appl. Mater. Interfaces* **2012**, *4*, 2570−2576.
(16) Xu, X.; Jia, J.; Yang, X.; Dong, S. *Langmuir* **2010**, *26*, 7627−7631.
(17) Lin, T.-H.; Lin, C.-W.; Liu, H.-H.; Sheu, J.-T.; Hung, W.-H. *Chem. Commun.* **2011**, *47*, 2044−2046.
(18) Nittmann, J.; Stanley, H. E. *Nature* **1986**, *321*, 663−668.
(19) Zheng, X.; Zhu, L.; Wang, X.; Yan, A.; Xie, Y. *J. Cryst. Growth* **2004**, *260*, 255−262.
(20) Pang, S.; Kondo, T.; Kawai, T. *Chem. Mater.* **2005**, *17*, 3636−3641.
(21) Lee, J.-H.; Kamada, K.; Enomoto, N.; Hojo, J. *Chem. Lett.* **2007**, *36*, 728−729.
(22) Pan, M.; Xing, S.; Sun, T.; Zhou, W.; Sindoro, M.; Teo, H. H.; Yan, Q.; Chen, H. *Chem. Commun.* **2010**, *46*, 7112−7114.
(23) Pan, M.; Sun, H.; Lim, J. W.; Bakaul, S. R.; Zeng, Y.; Xing, S.; Wu, T.; Yan, Q.; Chen, H. *Chem. Commun.* **2012**, *48*, 1440−1442.
(24) Agrawal, V. V.; Kulkarni, G. U.; Rao, C. N. R. *J. Colloid Interface Sci.* **2008**, *318*, 501−506.
(25) Zhang, J.; Meng, L.; Zhao, D.; Fei, Z.; Lu, Q.; Dyson, P. J. *Langmuir* **2008**, *24*, 2699−2704.
(26) Ilic, B.; Neuzil, P.; Stanczyk, T. *J. Mater. Sci. Lett.* **2000**, *19*, 193−195.
(27) Brankovic, S. R.; Wang, J. X.; Adžić, R. R. *Surf. Sci.* **2001**, *474*, L173−L179.
(28) Brankovic, S. R.; McBreen, J.; Adžić, R. R. *Surf. Sci.* **2001**, *479*, L363−L368.
(29) Van Brussel, M.; Kokkinidis, G.; Vandendael, I.; Buess-Herman, C. *Electrochem. Commun.* **2002**, *4*, 808−813.
(30) Van Brussel, M.; Kokkinidis, G.; Hubin, A.; Buess-Herman, C. *Electrochim. Acta* **2003**, *48*, 3909−3919.
(31) Papadimitriou, S.; Armyanov, S.; Valova, E.; Hubin, A.; Steenhaut, O.; Pavlidou, E.; Kokkinidis, G.; Sotiropoulos, S. *J. Phys. Chem. C* **2010**, *114*, 5217−5223.
(32) Tegou, A.; Papadimitriou, S.; Mintsouli, I.; Armyanov, S.; Valova, E.; Kokkinidis, G.; Sotiropoulos, S. *Catal. Today* **2011**, *170*, 126−133.
(33) Fang, J.; Ma, X.; Cai, H.; Song, X.; Ding, B. *Nanotechnology* **2006**, *17*, 5841−5845.
(34) Wang, C. H.; Sun, D. C.; Xia, X. H. *Nanotechnology* **2006**, *17*, 651−657.
(35) Li, Z.; Li, W.; Camargo, P. H. C.; Xia, Y. *Angew. Chem., Int. Ed.* **2008**, *47*, 9653−9656.
(36) Qin, Y.; Song, Y.; Sun, N.; Zhao, N.; Li, M.; Qi, L. *Chem. Mater.* **2008**, *20*, 3965−3972.
(37) Bai, X.; Gao, Y.; Zheng, L. *CrystEngComm* **2011**, *13*, 3562−3568.
(38) Dean, J. A. *Lange's Handbook of Chemistry*, 15th ed.; McGraw-Hill: New York, 1999.
(39) Mohl, M.; Kumar, A.; Reddy, A. L. M.; Kukovecz, A.; Konya, Z.; Kiricsi, I.; Vajtai, R.; Ajayan, P. M. *J. Phys. Chem. C* **2010**, *114*, 389−393.
(40) Liu, L.; Yoo, S.-H.; Park, S. *Chem. Mater.* **2010**, *22*, 2681−2684.
(41) Sarkar, S.; Sinha, A. K.; Pradhan, M.; Basu, M.; Negishi, Y.; Pal, T. *J. Phys. Chem. C* **2011**, *115*, 1659−1673.
(42) Xiao, J. P.; Xie, Y.; Tang, R.; Chen, M.; Tian, X. B. *Adv. Mater.* **2001**, *13*, 1887−1891.
(43) Murphy, C. J.; San, T. K.; Gole, A. M.; Orendorff, C. J.; Gao, J. X.; Gou, L.; Hunyadi, S. E.; Li, T. *J. Phys. Chem. B* **2005**, *109*, 13857−13870.
(44) Wang, L.; Li, H.; Tian, J.; Sun, X. *ACS Appl. Mater. Interfaces* **2010**, *2*, 2987−2991.
(45) Wang, D.; Li, T.; Liu, Y.; Huang, J.; You, T. *Cryst. Growth Des.* **2009**, *9*, 4351−4355.
(46) Imai, H. In *Biomineralization I*; Naka, K., Ed.; Springer: Berlin, 2007; Vol. *270*, pp 43−72.
(47) Lai, S. C. S.; Kleijn, S. E. F.; Öztürk, F. T. Z.; van Rees Vellinga, V. C.; Koning, J.; Rodriguez, P.; Koper, M. T. M. *Catal. Today* **2010**, *154*, 92−104.
(48) Chen, J.; Wang, M.; Liu, B.; Fan, Z.; Cui, K.; Kuang, Y. *J. Phys. Chem. B* **2006**, *110*, 11775−11779.
(49) Betowska-Brzezinska, M.; Uczak, T.; Holze, R. *J. Appl. Electrochem.* **1997**, *27*, 999−1011.
(50) Tremiliosi-Filho, G.; Gonzalez, E. R.; Motheo, A. J.; Belgsir, E. M.; Léger, J. M.; Lamy, C. *J. Electroanal. Chem.* **1998**, *444*, 31−39.
(51) Lima, R. B.; Varela, H. *Gold Bull. (Berlin, Ger.)* **2008**, *41*, 15−22.
(52) Huang, W.; Wang, M.; Zheng, J.; Li, Z. *J. Phys. Chem. C* **2009**, *113*, 1800−1805.
(53) Nagaraju, D. H.; Lakshminarayanan, V. *J. Phys. Chem. C* **2009**, *113*, 14922−14926.
(54) Yongprapat, S.; Therdthianwong, A.; Therdthianwong, S. *J. Appl. Electrochem.* **2012**, *42*, 483−490.
(55) Kwon, Y.; Lai, S. C. S.; Rodriguez, P.; Koper, M. T. M. *J. Am. Chem. Soc.* **2011**, *133*, 6914−6917.
(56) Trasatti, S.; Petrii, O. A. *Pure Appl. Chem.* **1991**, *63*, 711−734.
(57) Zope, B. N.; Hibbitts, D. D.; Neurock, M.; Davis, R. J. *Science* **2010**, *330*, 74−78.
(58) Yan, S.; Gao, L.; Zhang, S.; Zhang, W.; Li, Y.; Gao, L. *Electrochim. Acta* **2013**, *94*, 159−164.
(59) Wang, J.; Gong, J.; Xiong, Y.; Yang, J.; Gao, Y.; Liu, Y.; Lu, X.; Tang, Z. *Chem. Commun.* **2011**, *47*, 6894−6896.
(60) Yin, H.; Tang, H.; Wang, D.; Gao, Y.; Tang, Z. *ACS Nano* **2012**, *6*, 8288−8297.